CHEMISTRY & SUSTAINABILITY
CHEMSUSCHEM
ENERGY & MATERIALS

Supporting Information

The Nature of the Long-Lived Excited State in a Ni^{II} Phthalocyanine Complex Investigated by X-Ray Transient Absorption Spectroscopy

Jiyun Hong,[a] Matthew S. Kelley,[a] Megan L. Shelby,[a] Dugan K. Hayes,[b] Ryan G. Hadt,[b] Dolev Rimmerman,[a] Xiaoyi Zhang,[c] and Lin X. Chen*[a, b]

cssc_201800777_sm_miscellaneous_information.pdf

TA kinetics fitting

The analysis tool in OriginPro 8 was used to obtain time constants from the kinetics at 625nm, 705nm, and 730nm. The kinetic traces at 625nm and 705nm were fit to a bi-exponential equation, while the section of the trace at 730nm after 90 ps was fit to a mono-exponential equation. The data and the fit are shown in Figure S1 below. The obtained fitting parameters are summarized in Table S1.

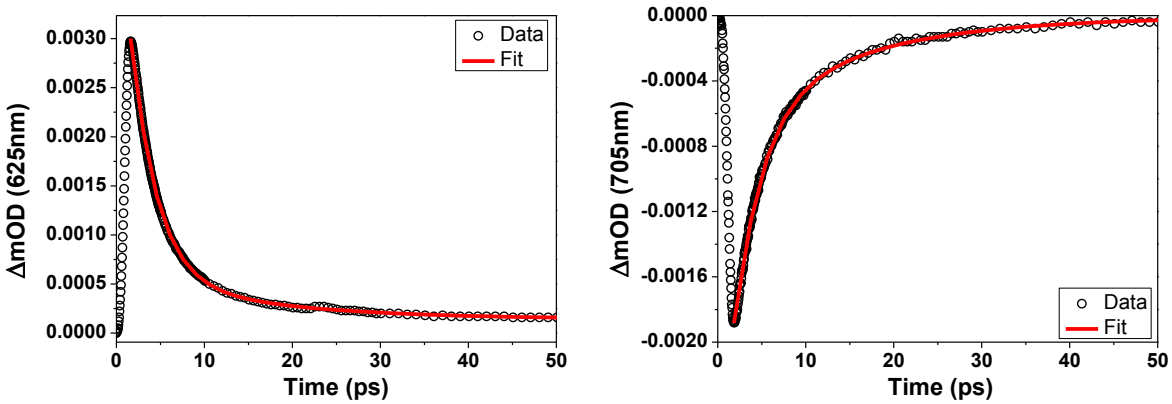

Figure S1. Kinetic traces and their fits at 625nm (left) and 705nm (right).

Table S1. Fitting parameters of the kinetic traces at 625nm, 705nm, and 730nm.

λ (nm)	τ_1 (ps)	A_1	τ_2 (ps)	A_2	R^2
625	15.56 ± 1.14	0.000479 ± 3.3e-5	2.878 ± 0.035	0.00444 ± 2.6e-5	0.999440
705	14.01 ± 0.54	-0.000721 ± 3.2e-5	3.066 ± 0.058	-0.00238 ± 2.3e-5	0.999440
730	680.8 ± 23.1	0.000910 ± 1.2e-5	-	-	0.976180

Baseline removal in the pre-edge region

The arctan-shaped baselines were first created using the Peak Analyzer feature in the OriginPro 8. The removal of the baselines reveals the actual shapes of the pre-edge features in ground state and the laser-on spectra. In Figure S2, it is apparent in the laser-on spectrum (red) that another small peak is appearing at lower energy, indicated by the blue arrow.

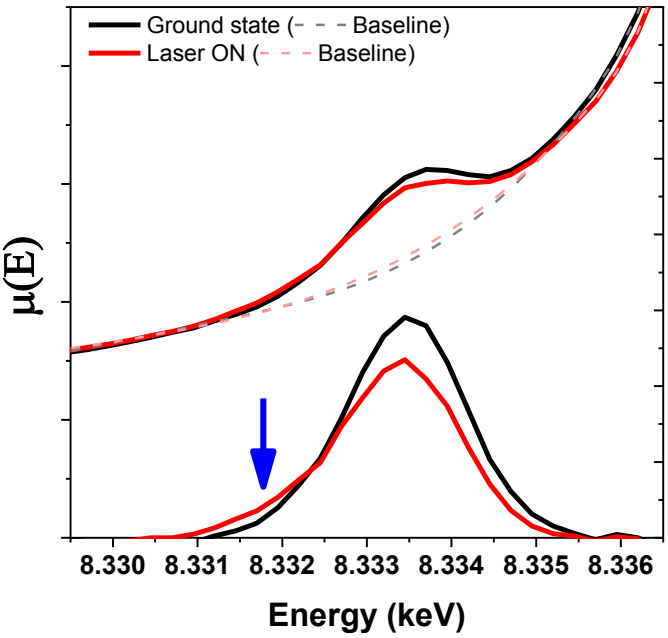

Figure S2. Pre-edge spectra of $NiPcOBu_8$ after base-line removal shows the apparent rise of a new feature, indicated by the blue arrow, upon laser-excitation.

Constructing the excited state spectrum: estimating the ground state fraction in the laser-initiated spectrum

The pure excited state spectrum was obtained by subtracting a fraction of remaining ground state contribution from the laser-initiated spectrum (at 100 ps delay) where the criteria for a pure excited state spectrum was the disappearance of the ground state 1s → $4p_z$ peak and the appearance of a new 1s → $4p_z$. The fraction of the ground state was determined to be about 82%. The excited state was extracted according to the equation (1),

$$\mu_{\text{excited state}}(\mathrm{E}) = \frac{\mu_{\text{laser-initiated}}(\mathrm{E}) - (82\% \times \mu_{\text{laser-off}}(\mathrm{E}))}{(1-82\%)} \qquad \text{Eq. (1)}$$

where μ is the X-ray absorption coefficient. The denominator is to normalize the intensity of the extracted excited state spectrum.

This subtraction method assumes that only two states are populated - the ground state and one excited state. This is reasonable as the optical TA data shows the mono-exponential decay kinetics of the ~680 ps-long lived excited state. The XTA time-delay scan measured at the top of the excited state 1s → $4p_z$ peak also exhibits mono-exponential decay kinetics. These results clearly indicate that there is only one excited state at 100 ps delay, validating the two-state model assumption in analysis.

To further verify that the ground state fraction is ~82% in the laser-initiated spectrum and that the extracted spectrum represents the pure excited state, the EXAFS fittings were conducted on the several spectra resulting from subtracting various ground-state fractions. Using the equation (1), but with different ground state fractions ranging from 90% to 40%, several “excited state” spectra were extracted. After the appropriate background removal and normalization, they were converted into k-space, and the quantitative EXAFS fittings were performed. The scattering paths used for the EXAFS fittings were generated using FEFF 6.0 in Artemis program based on the excited-state optimized triplet geometry obtained by the theoretical calculation. For consistency, the same k- and R-windows and the scattering paths were used for all the fittings. The resulting reduced chi-squared and R-factor values were compared to determined which spectrum gives the best fit with the optimized structure of the excited state $NiPcOBu_8$. Figure S3 below shows the reduced chi-squared and R-factor values plotted as a function of the ground-state fraction. The results indicate that the spectrum extracted from subtracting 83 ± 2% ground state fraction shows the best fitting results using the optimized structure calculated for the excited state.

Figure S4 shows the XANES region of the ground-state spectra and the series of the “excited-state” spectra extracted with varying amounts of ground state contribution. Qualitatively, 81-83% ground state fraction generates the most sensible-looking excited state spectra where the difference in the 1s → $4p_z$ transition peak is the largest while the pre-edge region has the most appropriate baseline shape.

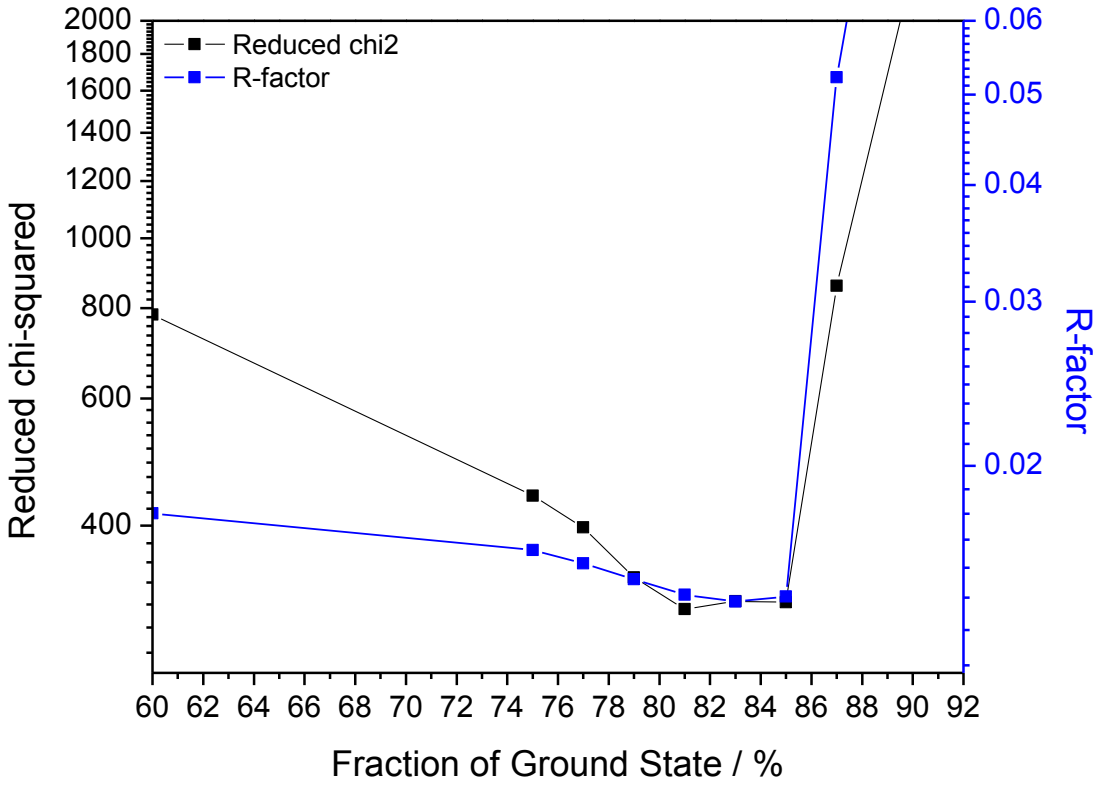

Figure S3. EXAFS fitting results of a series of excited-state spectra of $NiPcOBu_8$ constructed by subtracting varying amounts of ground state contribution from the laser-on spectra.

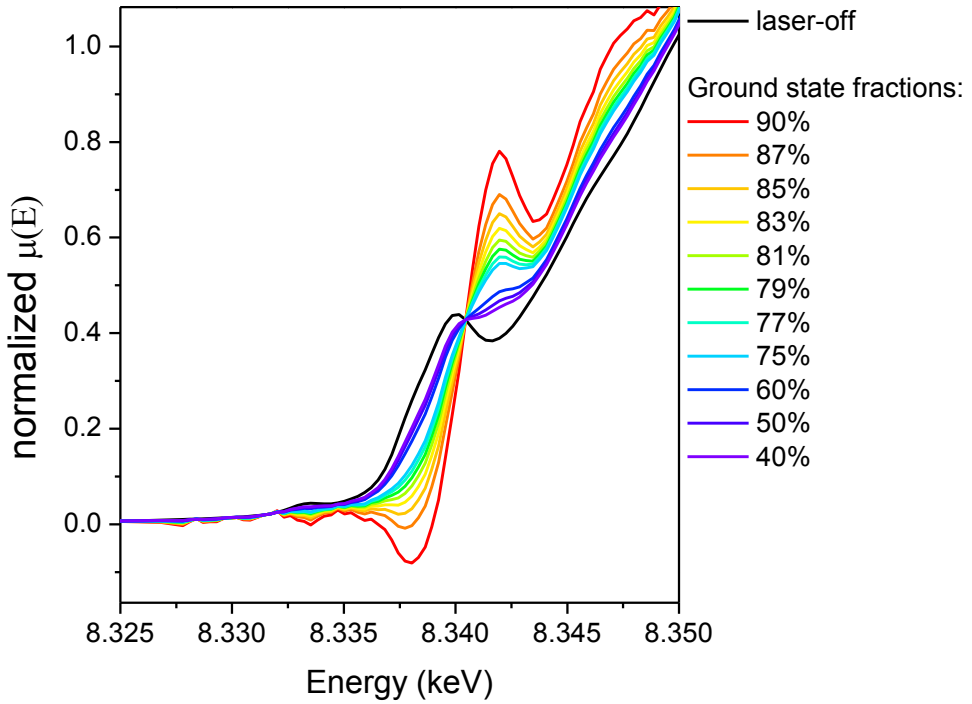

Figure S4. XANES region of the laser-off (ground state) and excited-state spectra of $NiPcOBu_8$ constructed by subtracting varying amounts of ground state contribution from the laser-on spectra.

Experimental data with standard error of the mean

The difference spectrum is plotted with standard error of the mean to demonstrate the statistical significance of the laser-induced changes observed experimentally.

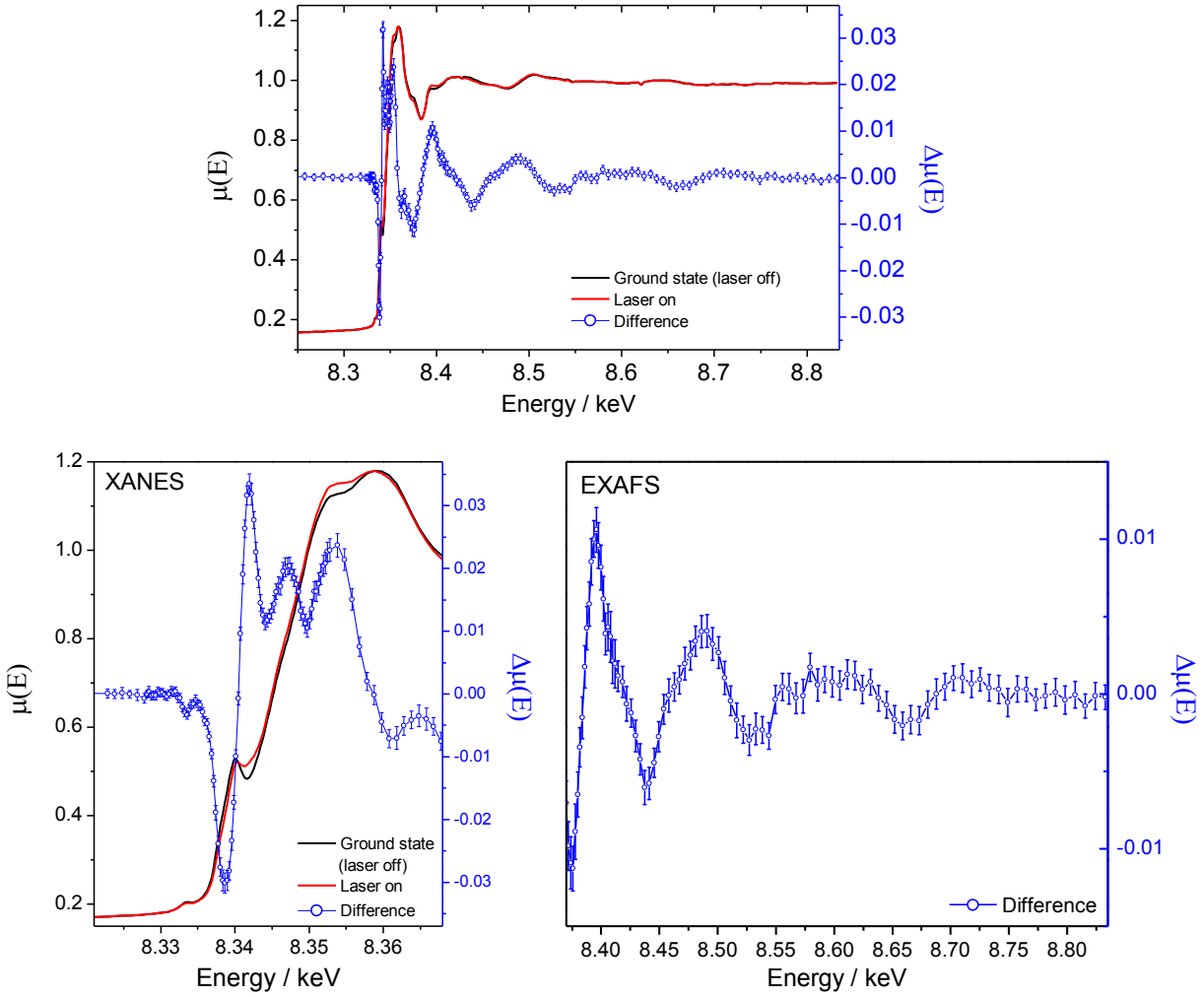

Figure S5. Top plot shows the entire XAS spectra of the ground state (black), laser-induced (red), and difference spectra with error bars (blue) for $NiPcOBu_8$. Bottom left plot shows the XANES region and the bottom right plot focuses on the EXAFS region. This set of data is an average of 88 scans. The error bars shown are 2.575 standard deviation of the mean (99% confidence interval).

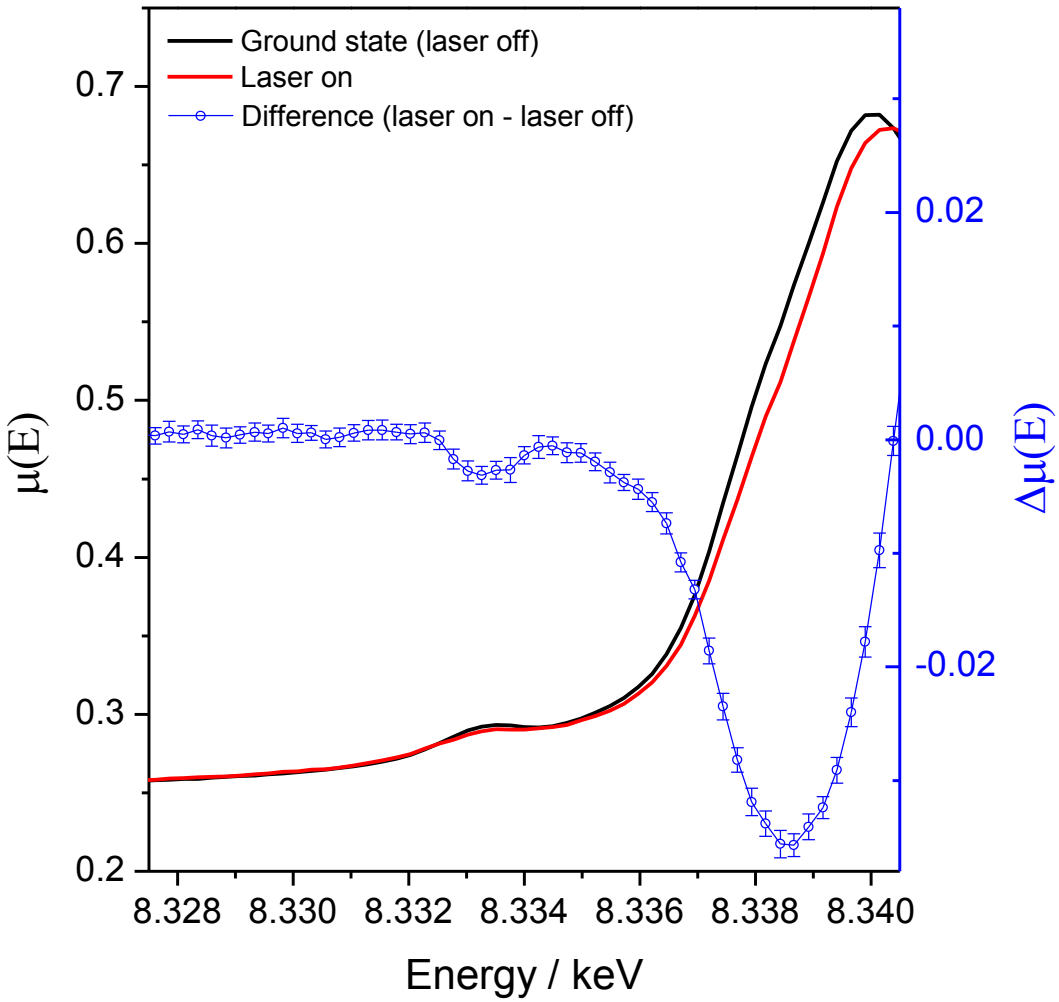

Figure S6. Pre-edge region of the ground state, laser-induced, and difference spectra with error bars for $NiPcOBu_8$. This set of data is an average of 42 scans that focused on the pre-edge region specifically with finer data point intervals. The error bars shown are 2.575 standard deviation of the mean (99% confidence interval).

Comparison between NiTMP and $NiPcOBu_8$ excited state XANES features

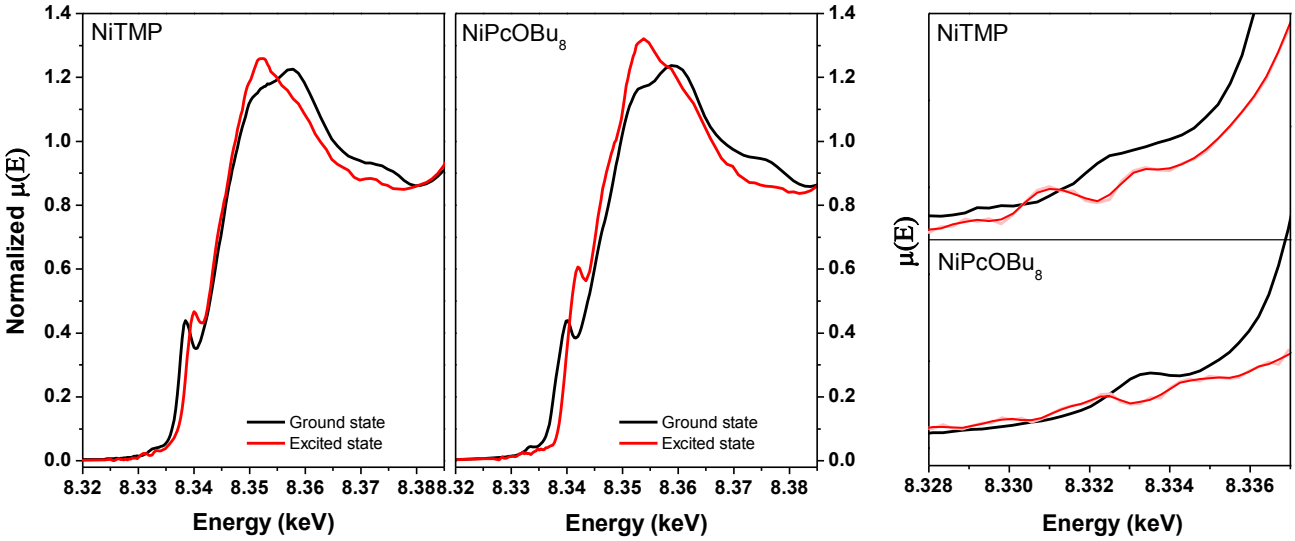

Figure S7. Comparison of the NiTMP and $NiPcOBu_8$ XANES. The NiTMP data is from our previous work[1–3]. The left and the middle show the XANES spectra of the ground state and ^{3}(d,d) (denoted as the excited state in the legend) in black and red, respectively. On the right is the enlarged pre-edge region of XANES spectra.

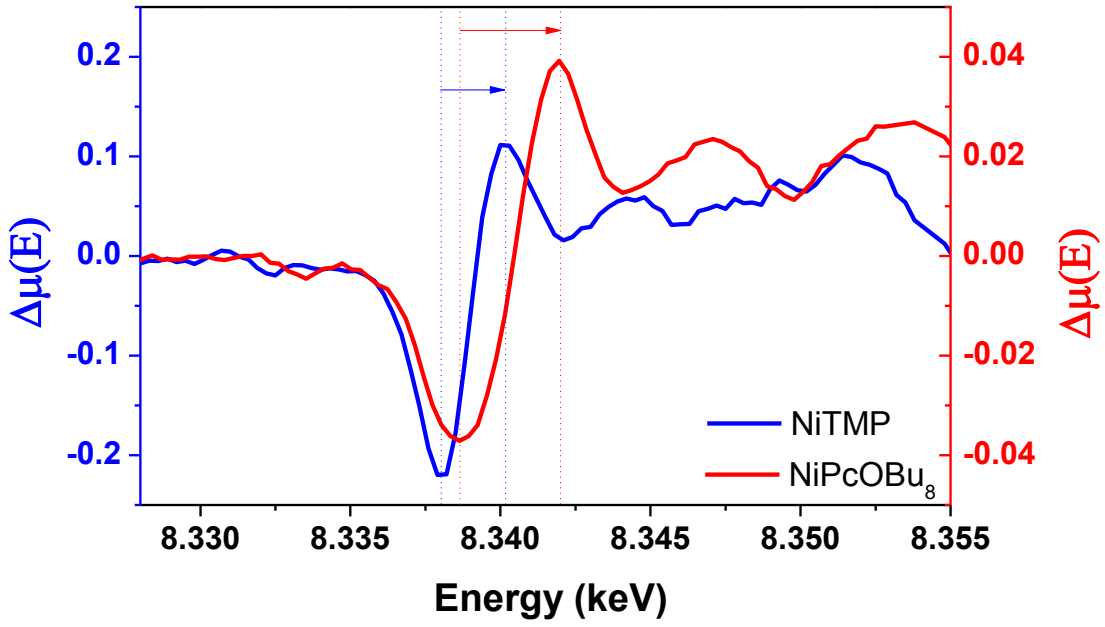

Figure S8. Comparison between the difference spectra of NiTMP (blue) and $NiPcOBu_8$ (red). The difference spectrum is the laser-off spectrum subtracted from the laser-on spectrum (probing the (d,d) state). The dashed lines and the arrows indicate the shifts in 1s → $4p_z$ peaks between the ground and excited states for NiTMP and $NiPcOBu_8$. The shift in energy is larger for $NiPcOBu_8$ compared to those of NiTMP. The energies were calibrated based on the Ni foil reference spectra.

Details of the EXAFS fitting

Data analysis of the ground state and excited state XTA spectra was performed using the Athena and Artemis program package[4,5]. All k-space and R-spectra are plotted with a k-weight of 3. To Fourier transform the k-space data into the R-space data, the k-space windows were chosen carefully to include the maximum number of oscillations available in the data with the minimum noise. The scattering paths used for the EXAFS fitting were generated with FEFF6.0 in Artemis using the NiPc crystal structure available on Cambridge Structural Database (CSD code: NIPHTC01) as a model structure[6] for the ground state data. For the excited state data, the optimized triplet geometry of $NiPcOMe_8$ was used as a model structure to generate the scattering paths.

The details of the fittings are displayed figures and table below. While multiple scattering paths were included, their contributions to the overall fitting were minor and only in the higher shell, hence only the single nitrogen and carbon scattering paths are described. The atoms used in the fitting are shown in Figure S11.

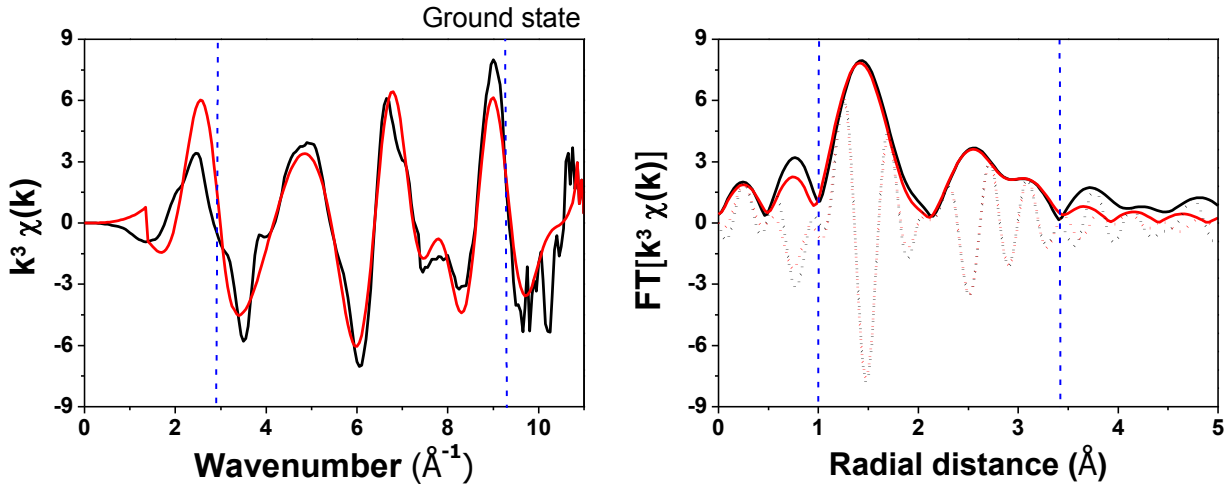

Figure S9. First- to third-shell fitting of the ground state EXAFS of $NiPcOBu_8$, shown in k-space (left) and R-space (right). The black line is the experimental data and the red line is the fit. In the the R-space EXAFS spectrum (right), the solid line is the magnitude R space, while the dotted line is the imaginary R space. The dashed blue lines are the k- and R-window ranges used for the fitting. The k-range used is 2.9 – 9.3 $Å^{-1}$ with a Hanning window with dk value of 0.2 $Å^{-1}$. The R-range used is 1.0 – 3.43 Å.

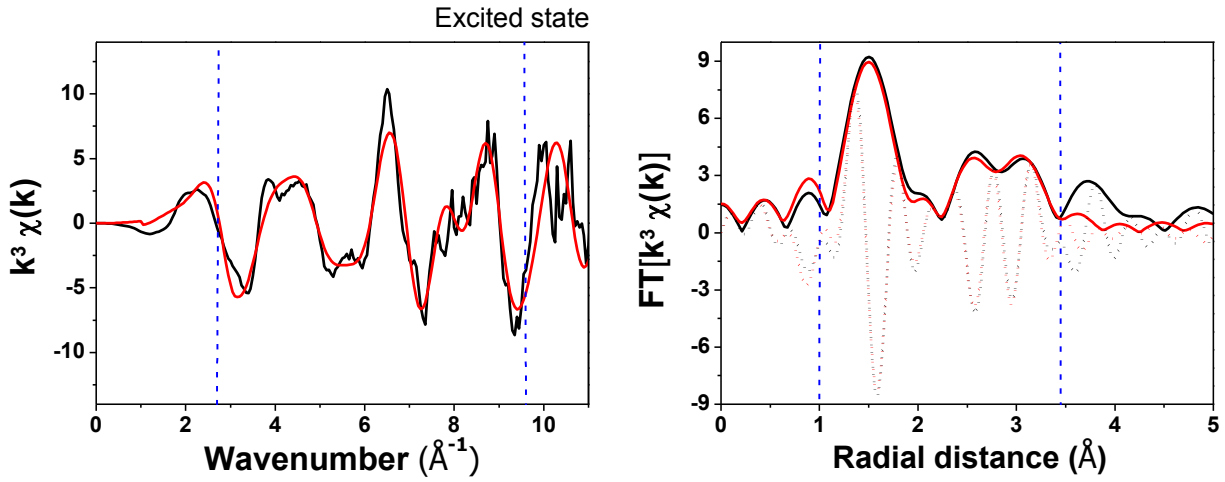

Figure S10. First- to third-shell fitting of the excited state EXAFS of $NiPcOBu_8$, shown in k-space (left) and R-space (right). The black line is the experimental data and the red line is the fit. In the R-space EXAFS spectrum (right), the solid line is the magnitude R space, while the dotted line is the imaginary R space. The dashed blue lines are the k- and R-window ranges used for the fitting. The k-range used is 2.9 – 9.6 $Å^{-1}$ with a Hanning window with dk value of 0.2 $Å^{-1}$. The R-range used is 1.0 – 3.45 Å.

Table S2. Extracted structural parameters of the EXAFS fitting of $NiPcOBu_8$ in its ground- and excited-state.

	Ground state			Excited state		
	ΔE = 7.1 eV, S_o^2 = 1.0			ΔE = 4.4 eV, S_o^2 = 1.0		
Atom-atom scattering path	N	R (Å)	σ^2 ($Å^2$)	N	R (Å)	σ^2 ($Å^2$)
Ni – N_p	4	1.89 ± 0.02	0.003	4	1.98 ± 0.03	0.002
Ni – C_α	8	2.93 ± 0.03	0.005	8	2.97 ± 0.03	0.001
Ni – N_b	4	3.27 ± 0.07	0.003	4	3.72 ± 0.01	0.001

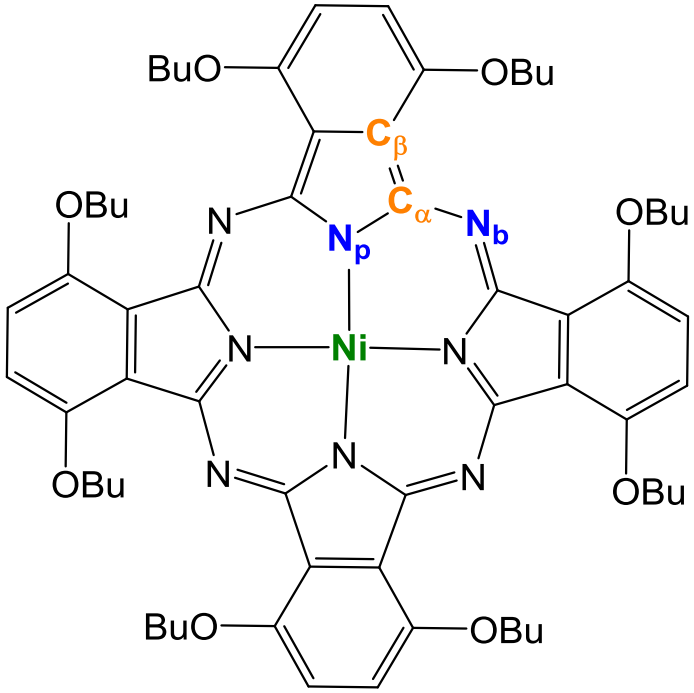

Figure S11. Atomic centers used in EXAFS data fitting.

References:

[1] M. L. Shelby, P. J. Lestrange, N. E. Jackson, K. Haldrup, M. W. Mara, A. B. Stickrath, D. Zhu, H. T. Lemke, M. Chollet, B. M. Hoffman, et al., *J. Am. Chem. Soc.* **2016**, *138*, 8752–8764.

[2] L. X. Chen, X. Zhang, E. C. Wasinger, K. Attenkofer, G. Jennings, A. Z. Muresan, J. S. Lindsey, *J. Am. Chem. Soc.* **2007**, *129*, 9616–9618.

[3] L. X. Chen, X. Zhang, E. C. Wasinger, J. V. Lockard, A. B. Stickrath, M. W. Mara, K. Attenkofer, G. Jennings, G. Smolentsev, A. Soldatov, *Chem. Sci.* **2010**, *1*, 642.

[4] B. Ravel, M. Newville, in *J. Synchrotron Radiat.*, **2005**, pp. 537–541.

[5] M. Newville, *J. Synchrotron Radiat.* **2001**, *8*, 322–324.

[6] L. Ruíz-Ramírez, A. Martínez, J.J. Sosa, J.L. Briansó, E. Estop, X. Alcobé y J.S.Chinchón. *Afinidad, XLIII*. **1986**, 404, 337-340.